Near Surface Geophysics, 2005, 21-31

A case study of two and three-dimensional inversion of dipole-dipole data: the Enfermarias Zn-Pb (Ag, Sb, Au) Prospect (Moura, Portugal)

P. Represas[1, 2], F. A. Monteiro Santos[1, 2*], A. Mateus[3, 4], J. Figueiras[3, 4], M. Barroso[4], R. Martins[4], V. Oliveira[5], M. Nolasco da Silva[5] and J.X. Matos[5]

[1] *Dpto Fisica da Faculdade de Ciências da Universidade de Lisboa, Ed. C8, Piso 6, Campo Grande, 1749-016 Lisboa, Portugal*
[2] *Centro de Geofísica de Universidade de Lisboa, Ed. C8, Piso 6, Campo Grande, 1749-016 Lisboa, Portugal*
[3] *Dpto Geologia, Faculdade de Ciências da Universidade de Lisboa, Ed. C6, Piso 4, Campo Grande, 1479-016 Lisboa, Portugal*
[4] *CREMINER, Faculdade de Ciências da Universidade de Lisboa, Ed. C6, Piso 4, Campo Grande, 1749-016 Lisboa, Portugal*
[5] *Instituto Geológica e Mineiro, Rua Frei Amador Arrais, 39 r/c, Apartado 104, 7802 Beja Codex, Portugal*

Received March 2003, revision accepted June 2004

ABSTRACT

The Enfermarias Zn-Pb(Ag, Sb, Au) prospect, located in the Moura-Ficalho region (Alentejo, Portugal), was intensively explored during 1980s. A drilling programme was successful, intersecting massive and disseminated sulphide mineralizations. The geological and geophysical data set available for Enfermarias is quite vast and comprises 13 borehole geological logs, as well as gravity, magnetic and resistivity data. In this paper, the dipole-dipole resistivity surveys are re-examined and interpreted using both 2D and 3D inversion to provide an interesting comparison of the two different approaches. Results from gravity data modelling and data from borehole logs are used as independent validity tests on the quality of the results.

The 2D and 3D models indicate a conductive overburden covering more resistive bedrock, which appears at a depth of 70–100 m in the western part of the profiles. Results obtained from 3D inversion, however, show a very clear separation of the most resistive domains in the two different bodies, whereas this separation does not appear in the 2D models. The 3D model also shows a higher degree of spatial continuity than the partial 2D models, which are, in general, richer in short-wavelength anomalies, and show a higher variation from profile to profile.

Comparison of the resistivity results with gravity in two coincident profiles reveals an excellent agreement between the main shallow features of both 2D and 3D models. This suggests that the resistivity model does indeed satisfy the main features of the available geological and geophysical data.

INTRODUCTION

The Enfermarias Zn-Pb(Ag, Sb, Au) prospect, located in the Moura-Ficalho region in Alentejo, Portugal (Fig. 1), was intensively explored by the Serviço de Fomento Mineiro (now the Instituto Geológico e Mineiro) during the 1980s (Oliveira and Matos 1992). The exploration was performed using a variety of geochemical, geophysical and geological methods, which included resistivity (dipole-dipole, mise-à-la-masse and rectangle), gravity and magnetic surveys, as well as detailed geological and soil geochemistry inspection of the terrain. Gravity and magnetic surveys were carried out to define drill targets. Resistivity surveys were made after drilling in order to characterize the orebodies.

Drilling was successful, intersecting massive and disseminated sulphide mineralization with Zn, Pb, Ag and Au contents up to 17.53%, 2.75%, 384 ppm and 3.2 ppm, respectively (Oliveira and Matos 1992). However, boreholes ore intersections were short and difficult to correlate from borehole to borehole, thus preventing a reliable assessment of the economic importance of the prospect. Despite this, and notwithstanding the promising ore grades found in the drill-cores, the potential of the rich and diverse geophysical data set collected at that time remained almost unexploited, except as a general guide for the emplacement of boreholes. In this work, we used the dipole-dipole data set to build two-dimensional (2D) and three-dimensional (3D) resistivity models of the prospect in an attempt to image both the orebodies and the general geological structure of the prospect, which is largely obscured due to the very adverse outcrop condi-

* fasantos@fc.ul.pt

tions. A 2D gravity model was also built, using borehole data (lithology and drill-core density measurements) as constraints, in order to assess the reliability of the resistivity models obtained.

Resistivity methods play an important role in applied geophysics, because their results constrain, in a fundamental way, the solution of many key issues in mineral exploration, groundwater monitoring, mapping of deep geological formations, geotechnical and environmental problems (e.g. Meju 2002). These methods are very versatile due to the great variety of available electrode arrays, the most widely used probably being the Schlumberger array, as well as Wenner, dipole-dipole and pole-dipole. The interpretation of resistivity data usually involves one-dimensional (1D) or 2D modelling, assuming, quite often, straightforward lithological and structural settings. However, geological systems are inherently 3D, and 3D inversion procedures appear to be the best approach for modelling the earth's

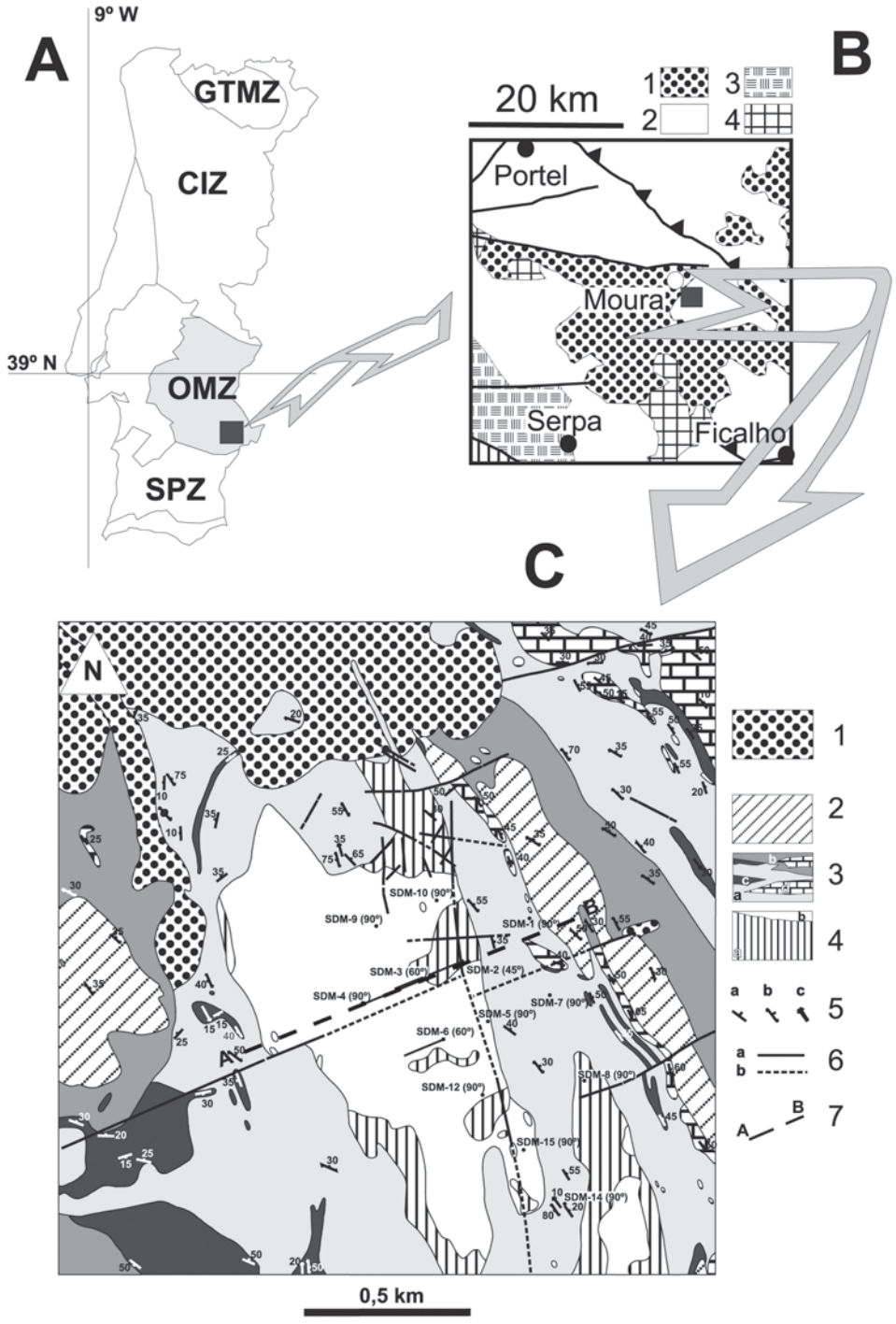

FIGURE 1
(a) Location of the Moura-Ficalho region, indicating the major geotectonic units of SW Iberia. CIZ: Central-Iberian Zone; GTMZ : Galicia – Trás-os-Montes Zone; OMZ : Ossa-Morena Zone; SPZ : South Portuguese Zone. (b) Schematic geological map of the Moura-Ficalho region. 1: Cenozoic sedimentary cover; 2: undifferentiated metasedimentary and metavolcanic rocks of Upper Proterozoic and Lower Palaeozoic ages; 3: gabbroic rocks of the Beja Igneous Complex (Lower Palaeozoic); 4: Late-Variscan granite intrusives. (c) Simplified geological map of the Enfermarias area with location of the boreholes performed (after Oliveira 1986, unpublished IGM internal report). 1: Cenozoic sedimentary cover; 2: Xistos de Moura Formation (Ordovician? – Silurian); 3: Volcanic-sedimentary Complex (Middle Cambrian? – Ordovician), a – felsic metavolcanic rocks, b – intermediate to mafic metavolcanic rocks, c – black cherts, d –marbles; 4: Dolomitic Formation (Lower Cambrian), a – metadolostones and other carbonate rocks, b – silico-ferruginous horizon; 5: Structural elements, a – strata direction and dip, b – schistosity, c – fold axis; 6: Fault trace, a – observed, b – inferred; 7: Geological cross-section (see Fig. 2).

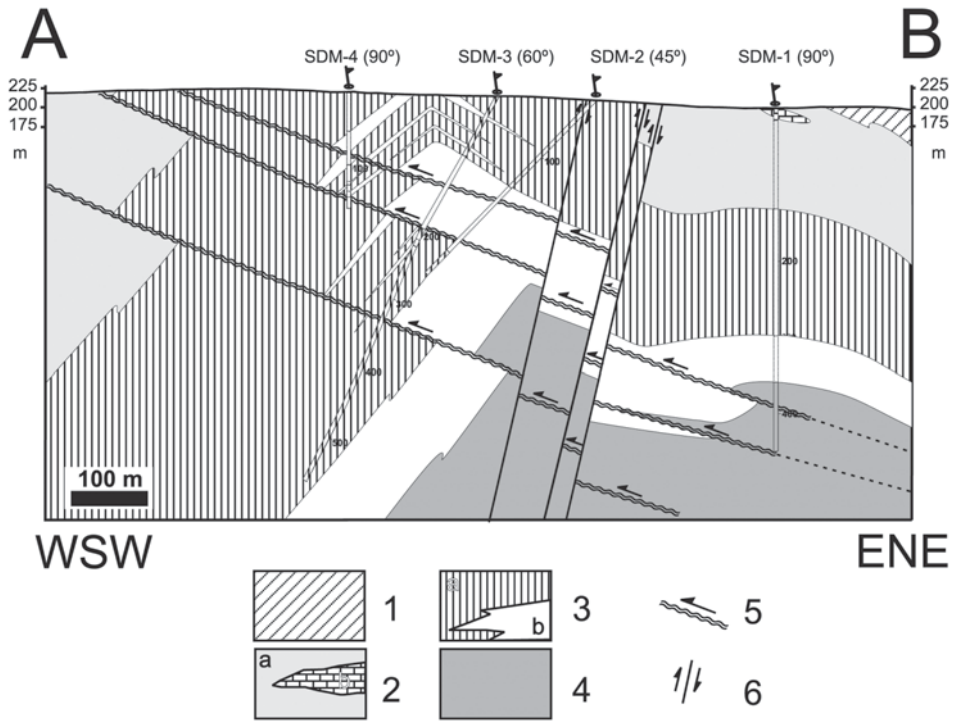

FIGURE 2
Geological cross-section indicated in Fig. 1(c), including data from boreholes SDM-1, SDM-2, SDM-3 and SDM-4 as well as those from field observations and measurements (after Barroso 2002; Martins 2003). 1: Xistos de Moura Formation (Ordovician? – Silurian); 2: Volcanic-sedimentary Complex (Middle Cambrian? – Ordovician), a – undifferentiated metavolcanic rock, b – marbles; 3 – Dolomitic Formation (Lower Cambrian), a – metadolostones and other carbonate rocks, b – metavolcanic rocks; 4: The Black Series (Upper Proterozoic); 5: Thrust zones (sheared metasomatic rocks); 6: Strike-slip fault zones.

subsurface, although such a sophisticated modelling technique can only be recommended and truly useful if the data set has the appropriate configuration. This means that the earth's subsurface must be densely sampled, preferably along the three spatial directions. It is assumed in this work that dipole-dipole arrays, performed in parallel and closely spaced profiles, produce such a dense, 3D sampling of the subsurface.

GEOLOGICAL SETTING

The Moura-Ficalho region is part of the Montemor-Ficalho Sector of the Ossa-Morena Zone, as defined by Oliveira *et al.* (1991) (Fig. 1b), and comprises four main geological formations, which from bottom to top are: (1) the *Black Series,* of Upper Proterozoic age, mostly composed of carbonaceous (sometimes graphitic) slates with thin black chert intercalations; (2) a *Dolomitic Formation* of Lower Cambrian age, essentially a thick succession of massive metadolostones with metavolcanic intercalations at the base and capped by a silico-ferruginous horizon, locally replaced by a meta-conglomerate; (3) a *Volcanic-Sedimentary Complex* of Middle (?) Cambrian – Ordovician age, a relatively thick series of bimodal metavolcanic rocks (with prevalence of rhyolitic suites) with interbedded strata and/or lenses of silicate-bearing marbles, carbonaceous or purple shales and cherts; and (4) the *Xistos de Moura Formation* of Ordovician (?) – Silurian age, a monotonous and thick sequence of slates, containing discontinuous levels of metapsammites, metavolcanics, and carbon-bearing shales and cherts. Further information on palaeontological, sedimentological and volcanogenic features of these formations are provided by Oliveira and Piçarra (1986), Oliveira *et al*. (1991), Piçarra (1991) and Ribeiro *et al*. (1991, 1997). All these rocks show important textural-mineral transformations developed either during the Variscan metamorphism (peaked at low amphibolitic facies conditions), or in the course of the subsequent retrogradation and/or hydrothermal activity, the latter triggered by the formation and reactivation of major fault zones with various kinematics. The effects of strong, although very heterogeneous, tectonic deformation can be observed at all scales, reflecting the strain partitioning and the distinct mechanical response of the rocks to the successive stress states developed during the Variscan Orogeny (Araújo 1995; Araújo and Ribeiro 1995).

At Enfermarias, the main structural features are mesoscopic NW-NNW-trending folds, with vergence towards the SW (locally known as the anticline-antiformal stacks of Enfermarias) and several WNW–ESE thrust zones, gently dipping (< 50°) towards the N-NE, and responsible for the over-thickening of some lithostratigraphical horizons and/or for their local strain increase. These structures, as well as all the geological formations referred to above, are indiscriminately affected by subvertical, strike-slip fault zones either in a N–S direction or ranging from NE–SW to ENE–WSW; their predominant kinematics, as inferred from the geometry and orientation of slickensides in mesoscopic planes of movement, are dextral and left-handed, respectively, indicating a stress field compatible with the one independently deduced elsewhere for Late-Variscan times (Marques *et al.* 2002).

At Enfermarias (Fig. 1c), the main outcropping rocks belong to the Volcanic-sedimentary Complex. Patches of metadolostones covered by the silico-ferruginous horizon, clearly belonging to the Dolomitic Formation, occur in a relatively narrow and elongated area along the anticline hinge zone. This major fold is

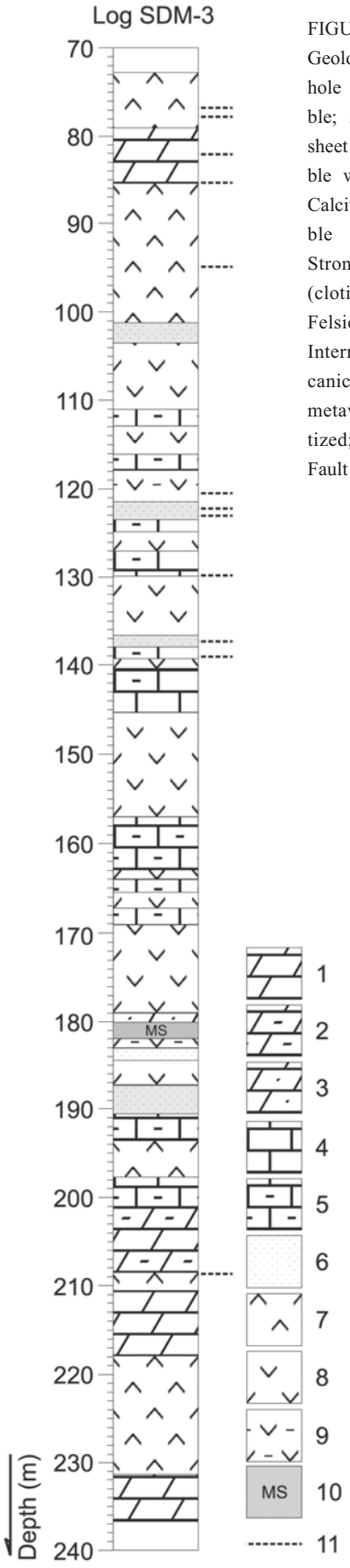

FIGURE 3
Geological well-log from borehole SDM-3. 1: Dolomitic marble; 2: Dolomitic marble with sheet silicates; 3: Dolomitic marble with tremolite/actinolite; 4: Calcitic marble; 5: Calcitic marble with sheet silicates; 6: Strongly metasomatized rock (clotite/serpentine + talc); 7: Felsic metavolcanics; 8: Intermediate-mafic metavolcanics; 9: Intermediate-mafic metavolcanics intensly chloritized; 10: Mineralization; 11: Fault zone.

asymmetrical and has its short limb cut by an important, N–S subvertical strike-slip fault zone. The remaining Lower Cambrian stratigraphical sequence (which hosts the disseminated and massive mineralizations) and the Proterozoic series do not outcrop and are known only from drilling.

Borehole data

Borehole data and part of the drill-cores (including whole-rock analyses for selected metals), were recently re-examined (Barroso 2002; Martins 2003). According to the available data, the rock sequence drilled at Enfermarias comprises metadolostones, different metavolcanic rocks (felsic to intermediate-mafic), with interbedded (decimetric) horizons of silicate-bearing marbles, and metasomatic rocks (mostly composed of chlorite/serpentine or of actinolite/tremolite and talc, the latter often developed along subhorizontal shear zones). Variscan deformation is responsible for the development of anisotropic fabrics, foliations and multiscale folding.

At the Enfermarias prospect, the oldest mineralization occurs as stacked massive centimetric ore lenses subparallel to the metamorphic foliation in strongly chloritized intermediate-mafic metavolcanics. This mineralization is mainly composed of unfractured sphalerite aggregates, parallel to the rock foliation, and strongly fractured pyrite grains with minor amounts of later galena, chalcopyrite, magnetite, arsenopyrite and sparse silver-bearing tetrahedrite. Massive centimetric aggregates of magnetite and pyrite were also identified, but always in strongly metasomatized rock domains adjoining thrust zones. Remobilization of the earlier sulphide ores has led to new disseminations and/or to the re-deposition of metals within rock domains where coeval fracturing was more intense. The development of coarse aggregates of pyrite + chalcopyrite ± pyrrhotite in fault breccias and late veins or bands with abundant hydrothermal quartz and chlorite, is clearly related to the evolution of the subvertical strike-slip fault zone, and records an independent copper-ore-forming system superimposed on the main, pre-existing, Zn-Pb(-Ag) geochemical halo.

The interpretative cross-section shown in Fig. 2 illustrates the geological framework of the site, considering borehole and surface data, while Fig. 3 shows the geological log of borehole SDM-3.

GEOPHYSICAL DATA

Gravity survey

Figure 4 shows the Bouguer anomaly map of the study area. Gravity stations were located at intervals of either 50 or 100 m, forming a grid that covers an area of 4 km^2. The data were collected in 1985 using a Worden gravity meter (IGM, unpublished internal report). A team of surveyors determined the location and elevation of the stations. A data error of 0.05 mGal was estimated. The elevation (Bouguer) correction of the observed gravity to sea-level was made assuming an average density of 2650 kg/m^3, considered to be a reasonable estimate of the Enfermarias geo-

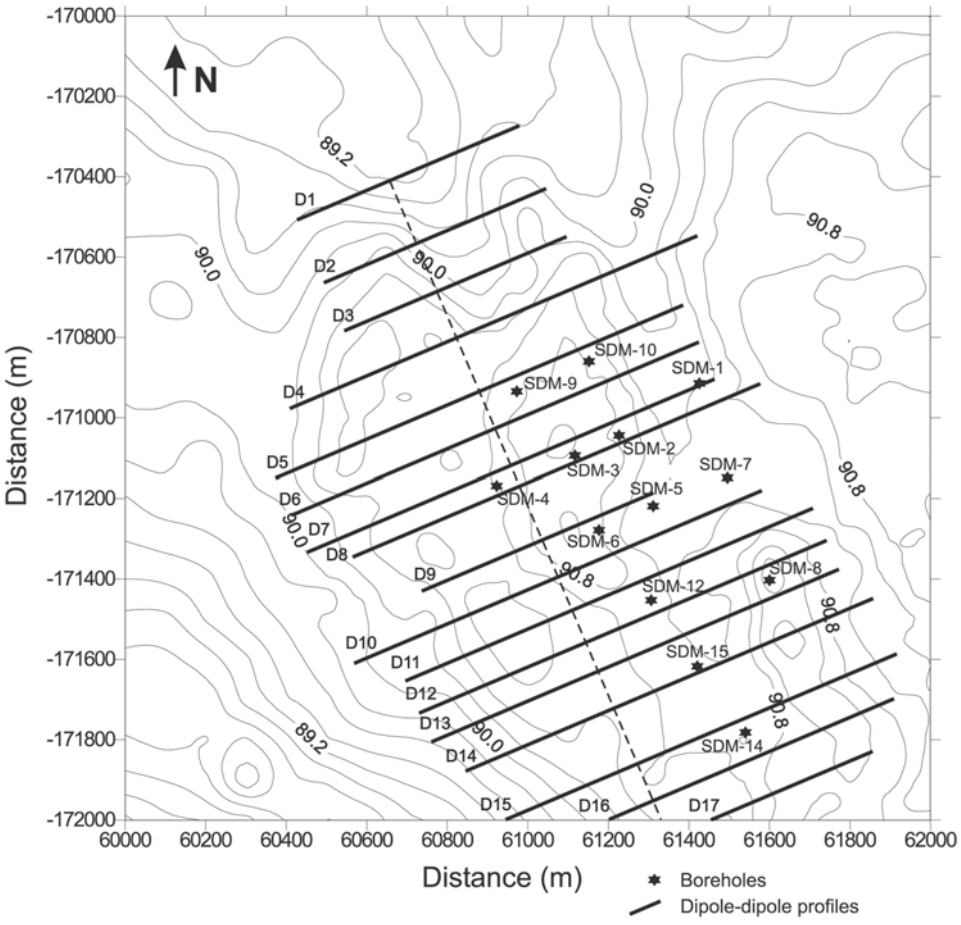

FIGURE 4
Bouguer anomaly map of the study area. Contour interval is 0.2 mGal. Solid lines are positions of dipole-dipole profiles. The dashed line represents the coordinate 0 m on the profiles.

logical background. Topographic corrections were not required due to the very low relief of the surveyed area.

The Bouguer anomaly map (Fig. 4) is characterized by two high-value, roughly oval-shaped anomalies at the centre and in the south-eastern part of the surveyed area, trending NNW–SSE to N–S, with a maximum Bouguer gravity value of 91.0 mGal. A third area with high gravity values is located on the eastern boundary of the area. The lowest Bouguer values (88.2 mGal) occur at the SW corner of the study area, where NW–SE trending contours indicate an approximately NE–SW gradient. An area characterized by low gravity values is also visible to the NW of the surveyed area, with values as low as 89.0 mGal.

Rock densities

Whenever possible, the rock densities used in this study were experimentally determined on drill-cores extracted from boreholes SDM-2 and SDM-3 (Table 1). It is assumed that these samples are representative of the main rock types, enabling the extrapolation of the density values obtained to domains that have not been drilled. The highest density value corresponds to mineralized (sulphide-enriched) domains, including massive ore lenses.

Dipole-dipole survey

The resistivity survey interpreted in this study comprised 17 dipole-dipole lines, covering an area of approximately 2.79 km^2. Figure 4 shows the location of the dipole-dipole lines. The corresponding apparent-resistivity pseudosections are shown in Fig. 5(a).

The dipole-dipole data were acquired in 1987–88, using a Scintrex resistivity meter. There is no information available on the errors associated with the data. The distance between electrodes is 50 m and most of the lines are divided into 28 dipoles, having a length of 1400 m. The exceptions are line D9, which has a length of 950 m divided into 19 dipoles, and lines D1, D2, D3 and D17, all 900 m long divided into 18 dipoles. The distance between dipole-dipole lines varies (Fig. 4), but averages about 100 m. The azimuth of the dipole-dipole lines is approximately N68°E.

RESULTS

Gravity profile

The regional component of the observed gravity cannot be properly determined from the data, because the Bouguer anomaly map is dominated by local anomalies. Therefore, it was decided

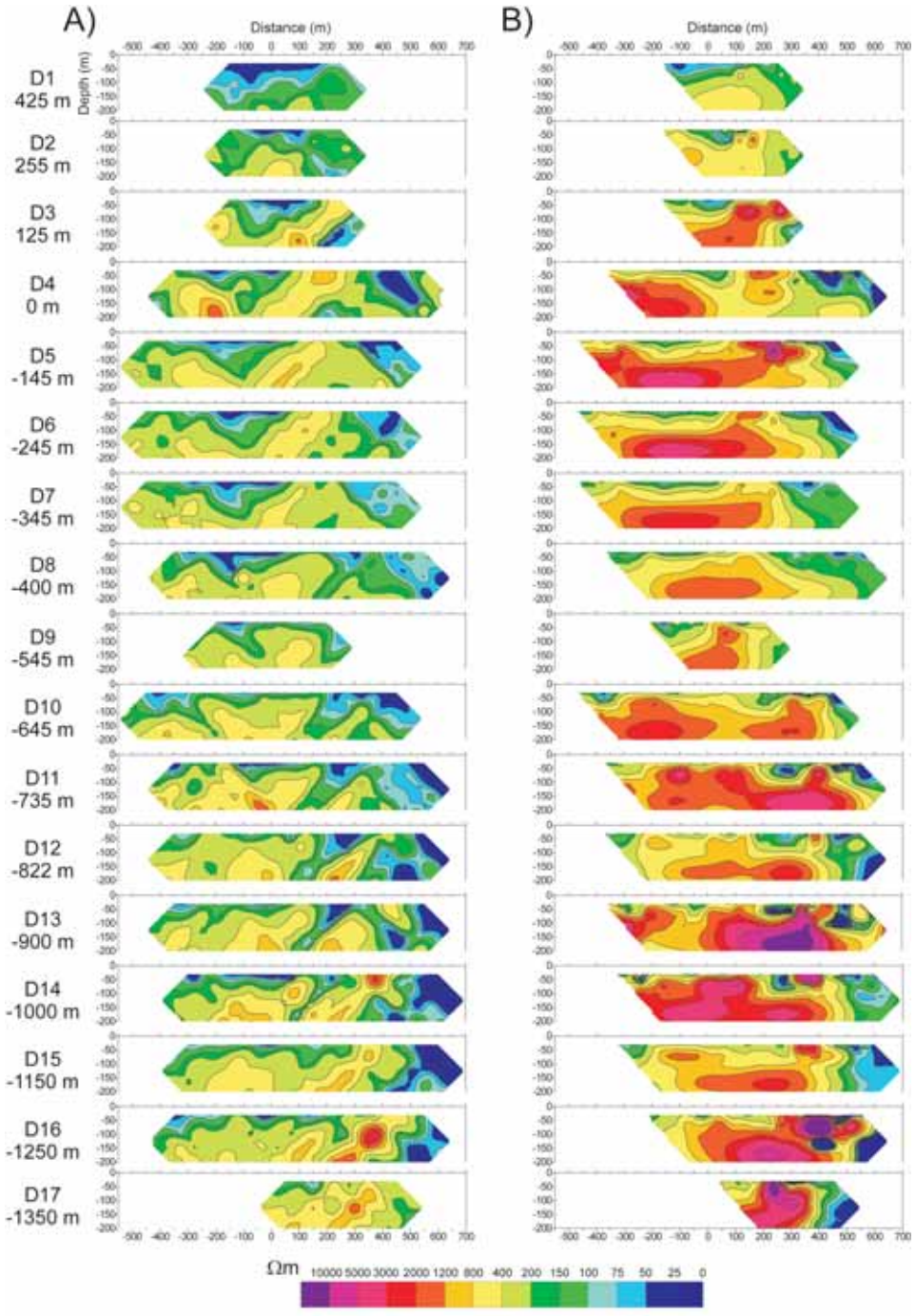

FIGURE 5
(a) Dipole-dipole field pseudo-sections. (b) Resistivity models obtained from 2D inversion of the field data.

to interpret the Bouguer anomaly instead of the residual component. Figure 6 shows the 2D gravity model for line D8, obtained by trial-and-error using Geosystem's commercial application WinGLink.

The global gravity anomaly has an evident three-dimensional character. The 2D approach is, however, justified in the context of this work because: (1) the main structures are very elongated in the NNW–SSE direction, and (2) the gravity results are used only for rough comparison with the resistivity models. A full interpretation of the gravity data is thus outside the scope of this work.

The gravity model was built considering the geological profile shown in Fig. 2 (Barroso 2002; Martins 2003). This profile, combined with the remaining geological information available (mainly from the boreholes), constrained the position of some interfaces of density contrast, as well as the approximate geometry of the main geological structures.

Gravity modelling started by assuming density values in the range of those measured on samples from boreholes SDM-2 and

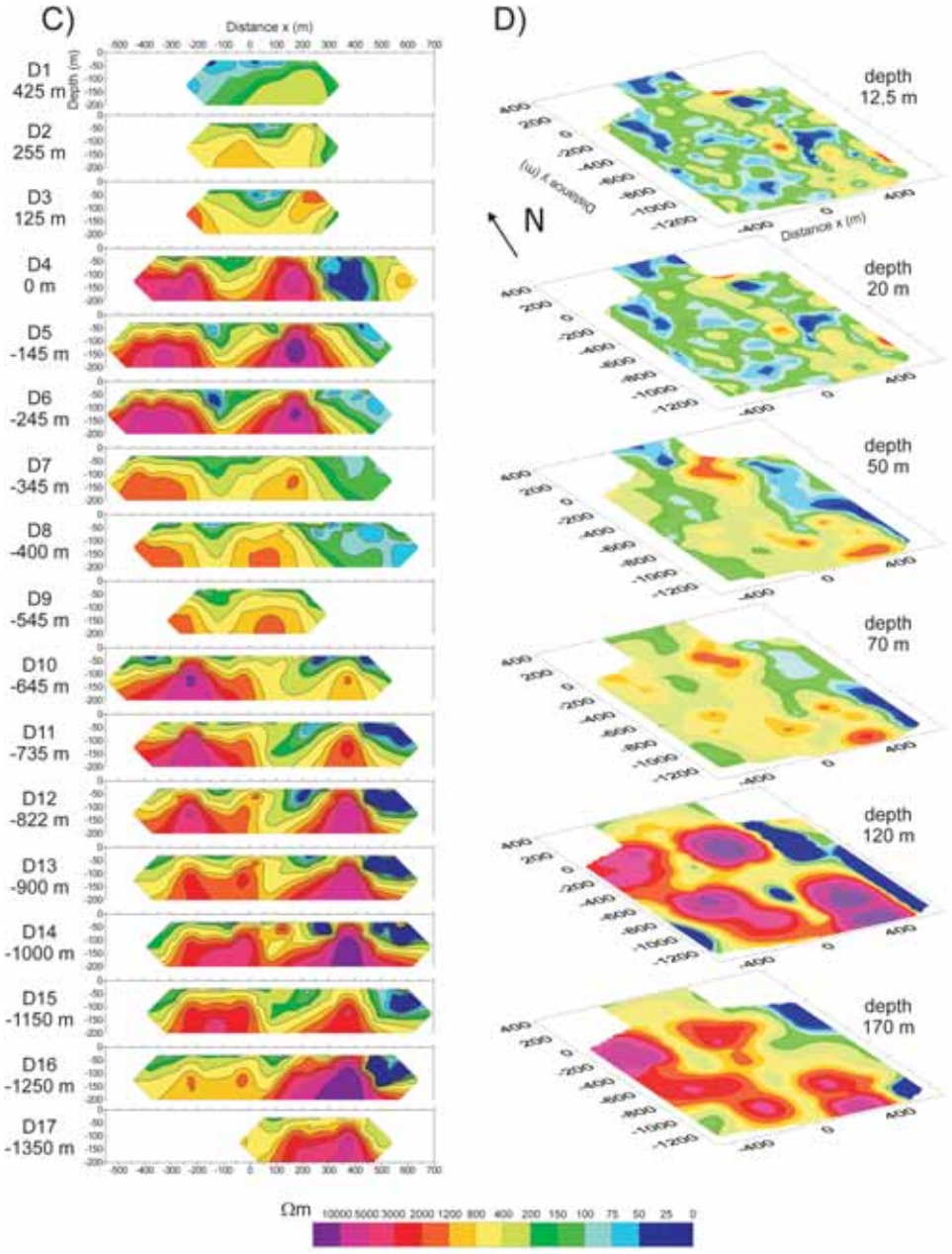

FIGURE 5
(c) and (d) Respectively vertical and horizontal slices of the resistivity model obtained from 3D inversion of the resistivity data set.

SDM-3 (Table 1). These values, together with minor details of the geometry of the blocks, were subsequently adjusted several times, and a final solution was chosen that provided an acceptable fit between the observed and the calculated gravity using geologically reasonable density values. Visual inspection shows that the misfit between data and model response is acceptable, and that the main features of the data are well represented in the model response. The difference between data and model response is generally within the data error bars.

For the model zone that is roughly coincident with the metadolostone sequence of the Dolomitic formation, a bulk density of 2650 kg/m^3 led to satisfactory results. The same was true for the metavolcanic sequence that forms the lower part of this geological formation, for which a bulk density of 2900 kg/m^3 was used. Comparison of these bulk density values with the data reported in Table 1 is not straightforward because, according to drill-core observations and to the performed measurements: (1) the metadolostone sequence displays a very heterogeneous distribution of sulphides and contains thin intercalations of marbles and of non-mineralized metavolcanics with lower densities (generally varying between 2500 kg/m^3 and 2700 k/m^3); and (2) the lower metavolcanic sequence is the preferential host of the massive sulphide ore lenses (with significantly higher densities). Note that the introduction of discrete and discontinuous, subparallel

TABLE 1

Measured density values in g/cm^3. A: Metadolostones of the Dolomitic Formation with some disseminated sulphides; B: Metadolostones of the Dolomitic Formation with abundant disseminated sulphides; C: Mineralized domains within the metavolcanic horizons of the Dolomitic Formation; D: Lower metavolcanic sequence of the Dolomitic Formation. Avg: average value; Med: median; Mod: mode; Min: minimum value; Max: maximum value

Formation	SDM-2 (146 measured samples)					SDM-3 (124 measured samples)				
	Avg	Med	Mod	Min	Max	Avg	Med	Mod	Min	Max
A	2.73	2.75	2.82	2.50	2.88	2.72	2.76	2.76	2.65	2.78
B	2.84	2.86	2.87	2.60	2.98	2.83	2.84	2.87	2.70	2.95
C	3.17	3.11	2.99	2.94	3.76	3.07	3.01	3.01	2.81	3.80
D	2.87	2.87	2.84	2.72	2.97	2.85	2.85	2.85	2.65	3.09

TABLE 2

Parametrization of the 2D dipole-dipole inversion. Ndp: number of data points; Npm: number of parameters (cells) of the model; Ni: number of iterations; error: misfit of the model response to data (%)

Profile	D1	D2	D3	D4	D5	D6	D7	D8
Ndp	64	64	64	134	134	134	134	134
Npm	117	117	117	207	207	207	207	207
Ni	3	5	4	4	5	4	3	3
Error	12.6	12.6	23.5	13.5	8.91	8.72	12.6	16.5

(Cont.)

Profile	D9	D10	D11	D12	D13	D14	D15	D16	D17
Ndp	64	134	134	134	134	134	134	134	64
Npm	117	207	207	207	207	207	207	207	117
Ni	3	4	4	3	7	5	4	6	5
Error	26.8	17.5	16.1	29.2	14.6	19.2	16.2	18.7	16.7

corridors of lower density (2400 kg/m^3) is needed in order to reduce the misfit of the model response (black lines in Fig. 6).

Variations in the basement depth and in the thickness of the major stratigraphical units can be detected by gravity measurements, provided that a density contrast exists between the main rock types. The model obtained does not preclude the presence of the secondary antiformal structure in the eastern part of the profile inferred from surface geological data. The abrupt western termination of the upper compartments concerned by this antiformal structure (coordinates 200 m to 300 m) is due to an important subvertical strike-slip fault zone which can be seen at the surface and in some of the boreholes; its dip agrees with surface geological measurements.

The main positive anomaly of the profile is ascribable to the presence of sulphide-rich metavolcanic rocks that are much denser (2900 kg/m^3) than the surrounding rocks. The decrease in gravity values towards the east and the west is due to the presence of thick shallow sequences of low-density rocks; conversely, shallow, relatively high-density rocks give rise to the increasing gravity values of the eastern limit of the profile.

The shallow structures of the gravity model are quite well constrained. Conversely, some of deep features of the gravity model (depths greater than 200 m) are not well constrained and other solutions are possible; for example, the misfit is not substantially altered when the dip of the subvertical strike-slip fault zone is changed by ±10°.

2D resistivity dipole-dipole inversion

Figure 5(b) shows the results of models obtained from 2D inversion of the dipole-dipole lines. The inversion was performed using a non-linear smoothness-constrained algorithm (Sasaki 1989). The main characteristics of the parametrization used in the inversion of each profile are given in Table 2.

As the data errors are not known, the quantity,

$$error = \frac{100}{N}\sum_{i=1}^{N}\frac{|r_{obi} - r_{cali}|}{r_{obi}},$$

was used to quantify the misfit between data and model responses, where N represents the number of data points, and r_{ob} and r_{cal} are the values of measured and calculated apparent resistivity values. The data inversion was carried out with different damping factors in the range 0.1–0.3. Several initial homogeneous resistivity values were tested for each inverted line, in order to achieve the lowest error. The final models were obtained with the following initial resistivities: 200 Ωm for lines D2, D3, D4 and D17; 100 Ωm for lines D1, D7, D9, D13 and D16; 50 Ωm for lines D5, D6, D8 and D10 and 25 Ωm for lines D11, D12, D14 and D15. The time required to perform these inversions, calculating full derivatives at each iteration, varies between 45 min and 3 hours, using an Intel Pentium 4 1.8 GHz processor with 512 MB of RAM.

For a good convergence, the misfit error values should be of the same order as the data error. The highest value is 29.2%, and was found on line D12 and the lowest is 8.72% on line D5. Most of the models have errors between 13% and 19%. These values seem acceptable, given the high resistivity contrasts shown in the apparent-resistivity pseudosections.

It can be seen from the models in Fig. 5(b) that there is a significant difference between the northern (lines D1 to D9) and the southern (lines D10 to D17) parts of the study area. In the northern part, the models suggest a high-resistivity structure, with values greater than 1200 Ωm, at a depth of 70–100 m and centred approximately at coordinate –100 m. Towards the south, this resistive structure appears to split into two similar structures, centred approximately at coordinates, –200 m and 300 m. To the south of line D15, the high-resistivity structure is no longer detectable in the western part of the profiles, probably because these lines do not sample it. A zone of low resistivity (25–100 Ωm) can be observed in the eastern part of all profiles. In the transition between the high- and the low-resistivity zones, there is a steep decrease in the resistivity values, most probably caused by the presence of the subvertical strike-slip fault zone.

3D resistivity dipole-dipole inversion

The 3D inversion was made by considering the three-dimensional data set resulting from all 17 dipole-dipole lines (a total of 342 source locations and 2181 data measurement points were used). The grid used (143×122×15 nodes in the N68°E, N22°W and downward directions, respectively) covers an area of 2700×2775 m^2. Along the x-axis (parallel to the dipole-dipole profiles), a 12.5 m mesh spacing was fixed in the area covered by data. At the boundaries, the mesh was enlarged until it reached a spacing of 200 m. Along the y-axis, a 15.5 m to 24 m wide mesh was used, and the spacing was also increased at the boundaries until it reached 200 m. In the downward direction, the mesh spacing Δz increased according to the exponential law $\Delta z = \Delta z_m \exp(0.2lz)$, where Δz_m represents the thickness of the uppermost hexahedral element (15 m in this case) and lz is the vertical level of the element. The model was parametrized in 2774 cells of unknown resistivity. The initial starting model was defined as a homogeneous medium with a resistivity of 100 Ωm. The 3D inversion was performed using the smoothness-constrained algorithm proposed by Sasaki (2001), with a damping factor of 0.6. The forward modelling was based on the finite-element approach (Pridmore 1978). The derivatives were calculated using the approach proposed by Loke and Barker (1996). After 10 iterations, the misfit error attained in the inversion was 15%. The CPU time required to perform one iteration was 10 hours on an Intel Pentium 4 1.8 GHz processor with 512 MB RAM.

Vertical slices of the 3D model obtained from inversion of the dipole-dipole data set are shown in Fig. 5(c). The slices shown correspond to the location of the field lines to assist in the comparison with the results obtained with 2D inversion. Six horizontal cross-sections of the model are shown in Fig. 5(d). These images reveal the presence of resistive bedrock lying under a more conductive overburden. The model also shows two high-resistivity structures (values greater than 1200 Ωm), at coordinates x= –300 and 150 m to the north of line D9. To the south of this line the model suggests an eastward 100–200 m shift of the resistive structures. As in the 2D models, a low-resistivity area can be detected in the eastern part of the area surveyed.

DISCUSSION

Firstly, it can be observed that both types of model (2D and 3D) indicate a conductive overburden covering more resistive bedrock in the western part of the profiles. The most significant differences between the models obtained with 2D and 3D approaches are observed between coordinates –150 m and 300 m approximately. Results of the 3D model show a very clear separation of the most resistive domains in two different bodies, whereas this separation does not appear in the 2D models. Also, the maximum resistivity values of the 3D model are significantly higher than those found in any of the 2D models. 3D results appear to be more realistic, taking into account the probable nature of the geological formations (non-weathered Lower Cambrian rocks).

The second aspect concerns the spatial continuity of the main structures, particularly in profiles D10–D17. The 3D global model shows a higher degree of continuity than the partial 2D models, which are, in general, richer in short wavelength anomalies and show a higher variation from profile to profile. This can be interpreted in the sense that the 2D inversion is more vulnerable to non-uniqueness problems, due to the three-dimensional character of the geological structure under survey.

The shallow low-resistivity feature running from north to south in the 3D model (between coordinates x=200 m and 300 m in the northern profiles and coordinates x=50m and 150 m in the southern profiles) needs a geological explanation. Its location in the model coincides approximately with a tectonic structure characterized by a wide, brecciated, porous and partly mineralized fault gauge, which would explain the low-resistivity values. Its apparent eastward shift between profiles D9 and D10 suggests the presence of a transverse fault, for which no field

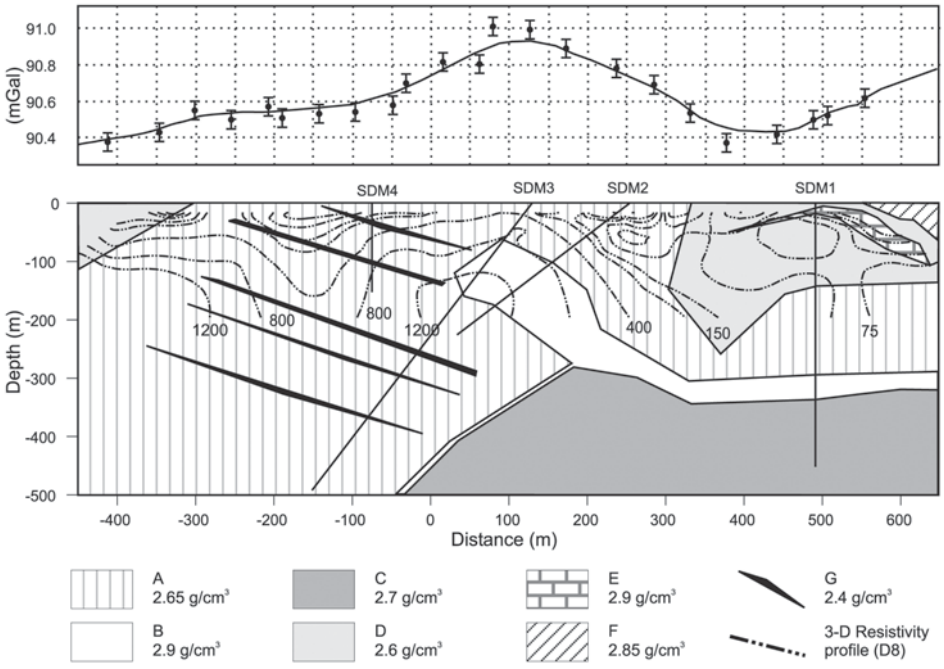

FIGURE 6
Gravity model derived from well-log and geological information. The geometry and depth of some interfaces are locally constrained by wells drilled either on or close to the line. The dashed lines (values in Ωm) represent the cross-section of the 3D resistivity model coincident with the gravity line (profile D8 of Fig. 4). A: Metadolostones and other carbonate rocks. B: Metavolcanic rocks. C: The Black Series. D: Undifferentiated metavolcanic rocks. E: Marbles. F: Xistos de Moura Formation. G: Thrust zones (sheared metasomatic rocks).

evidence exists. The left-handed subvertical fault parallel to profile D8, which has been recognized in the field, cannot be responsible for the observed shift because geological mapping shows that its displacement is necessarily much lower than the 150–200 m displacement shown by the 3D model. The most plausible explanation for the observed 3D model features is that the N–S-trending fault belongs to a hidden en-echelon system, so that the low-resistivity feature seen to the north of profile D9 is not the one seen to the south of it. As can be seen in Fig. 1(c), the fault zone corresponding to this latter feature is easily followed in the field; the northern fault may be represented by the small stretch recognized immediately to the north-east of the SDM-9 borehole (note again that the study area is almost flat and devoid of outcrops).

Results from the different models, either 2D or 3D, show that the resistivity increases with depth to values that may be higher than 10 000 Ωm. Comparison of these results with the available geological data strongly suggests that this high-resistivity domain corresponds to the Lower Cambrian rocks, irrespective of their lithological nature. The values found in the models suggest that these rocks are relatively dry and non-weathered; indeed, drill-core observation reveals that no weathering effects are visible below circa 80 m. Drill-core observation also reveals that the Lower Cambrian sequence hosts the sulphide mineralization and is cut by relatively frequent, although quite thin, intercalations of strongly metasomatized rocks essentially composed of sheet silicates. The expected low-resistivity values corresponding to both are, however, absent from the models. This is due to a number of reasons. The metasomatized rocks are too thin to be resolved by the model, but their presence must lower the overall resistivity of the geological formations they cut through; note that they had to be explicitly considered in the gravity model to achieve an acceptable fit to the gravimetric data while preserving reasonable density values for the remaining rockbodies. Similar reasons may, in part, justify the lack of low-resistivity domains due to mineralization. Massive sulphide lenses exist, but are very thin, probably have short horizontal extension, and are mostly composed of sphalerite, which is a relatively poor conductor. Moreover, most of the total sulphide mineralization is disseminated, not massive, and consists of non-connected sulphides (essentially pyrite and sphalerite), which, even if they are good conductors or semi-conductors (such as pyrite), will not contribute to a lowering of the bulk resistivity because of their weak electrical connectivity. Note also that the most important metal anomalies were intersected by borehole SDM-3 and appear to be confined to the hinge of the Enfermarias anticline-antiformal stack.

The resistivity gradients which appear in the easternmost part of the 2D models also exist, almost identically, in the 3D model. This domain of very low-resistivity values correlate quite well with variably weathered metavolcanic rocks and schists belonging to the uppermost stratigraphical levels in the area.

A rough cross-validation of the electrical models obtained can be performed through examination of their relationship with the gravity results in two coincident profiles (the dipole-dipole profile D8 of the 3D model and the gravity profile AB shown in Fig. 1c). It is known that the solution of the gravity problem is highly ambiguous. However, the use of the geological information available allowed us to constrain a few parameters of the model. The two best models estimated from gravity and resistivity data are superposed in Fig. 6, revealing an outstanding agreement between the main features of both models for the same

depth range (0–200 m). The correlation between resistivity and density distributions is quite evident, namely: (1) the low resistivity at coordinates 200 m and 300 m can be associated with the presence of the fault and (2) the high resistivities at deeper parts correlate very well with the weathered metavolcanic rocks. The same general correlation can be observed when comparing Figs 4 and 5(d).

In general, the geophysical models confirm some of the geological hypotheses, at least within the resolution limits of each method. The loss of resolution of the resistivity data with depth does not allow the confirmation of the hypothesized presence of some geological structures. The thin sheets of metasomatized rocks are an example of such unconfirmed structures. The gravity data set has a limited sensitivity to these structures but the fact is that their presence in the model allows a better agreement between data and model response.

SUMMARY AND CONCLUSIONS

This work describes the interpretation of a resistivity survey carried out in an ore prospect located in the Moura-Ficalho region. The amount of data collected in that area is vast, comprising resistivity data, borehole logs, gravity and magnetic data.

The inversions of apparent-resistivity data collected along 17 parallel dipole-dipole profiles using 2D and 3D approaches show compatible electrical-resistivity distributions, but some differences associated with inappropriate model representation are revealed. The 3D inversion of the whole data set allows the calculation of a more coherent and less ambiguous model. As expected, the 3D inversion is much more time consuming than the 2D inversion. Nevertheless, the use of this interpretative technique seems perfectly justified in this case.

The borehole geological information was, at first, used to impose constraints on the 2D modelling of a gravity profile across the main structures, which was subsequently superposed on the calculated resistivity models. The excellent agreement obtained indicates that the 3D resistivity model does indeed satisfy the main features of the available geological and geophysical data.

REFERENCES

Araújo A. 1995. *Estrutura de uma geotransversal entre Brinches e Mourão (Zona de Ossa-Morena): implicações na evolução geodinâmica da margem sudoeste do Terreno Autóctone Ibérico*. PhD thesis, Universidade de Évora, Portugal.

Araújo A. and Ribeiro A. 1995. Tangential transpressive strain regime in the Évora-Aracena Domain (Ossa Morena Zone). *Buletin Geológico y Minero* **106**(2), 111–117.

Barroso M. 2002. *Caracterização mineralógica e textural das mineralizações sulfuretadas da jazida de Enfermarias (Moura, Portugal)*. MSc thesis, Universidade de Lisboa, Portugal.

Loke M.H. and Barker R.D. 1996. Practical techniques for 3D resistivity surveys and data inversion. Geophysical Prospecting **44**, 499–523.

Marques F.O., Mateus A. and Tassinari C. 2002. The Late-Variscan fault network in Central-Northern Portugal: a re-evaluation. *Tectonophysics* **359**, 255–270.

Martins R. 2003. *Caracterização dos processos metassomáticos correlativos da recristalização e deposição de sulfuretos na jazida de Enfermarias (Moura, Portugal)*. MSc thesis, Universidade de Lisboa, Portugal.

Meju M.A. 2002. Geoelectromagnetic exploration for natural resources, case studies and chalanges. *Surveys in Geophysics* **23**, 133–205.

Oliveira J.T., Oliveira V. and Piçarra J.M. 1991. Traços gerais da evolução tectono-estratigráfica da Zona de Ossa Morena em Portugal. *Cuad. Lab. Xeol. Laxe* **16**, 221–250.

Oliveira V. and Matos J. 1992. Enquadramento geológico-mineiro da Jazida de Enfermarias (Faixa Magnetítico-Zincífera, Sector SW da Zona de Ossa-Morena). *VII Reunion del Grupo de Ossa-Morena, Cáceres, España, Libro de Resúmenes* (eds I. Rábano & J.C. Gutiérrez-Marco), pp. 114–115.

Oliveira V. and Piçarra J.M. 1986. Litoestratigrafia do Anticlinório de Moura-Ficalho. *Maleo* **13**, 33.

Piçarra J.M. 1991. Descoberta de graptólitos silúricos em liditos da formação dos Xistos de Moura, Maciço de Évora-Beja: implicações tectonoestratigráficas. *XI Reunión de la geología del Oeste Peninsular*, pp. 34–35.

Pridmore D.F. 1978. *Three-dimensional modelling of electrical and electromagnetic data using the finite element method*. PhD thesis, University of Utah, USA.

Ribeiro M.L., Mata J. and Piçarra J.M. 1991. Vulcanismo bimodal da região de Ficalho: características geoquímicas. *Comun. Serv. Geol. Portugal* **78**(2), 75–85.

Ribeiro M.L., Munhá J., Mata J. and Palácios T. 1997. Vulcanismo na Zona de Ossa Morena e seu enquadramento geodinâmico. In: *Estudos Sobre a Geologia da Zona de Ossa-Morena (Maciço Ibérico)*. Livro de Homenagem ao Prof. Francisco Gonçalves, Évora, Portugal, pp. 37–56.

Sasaki Y. 1989: Two-dimensional joint inversion of magnetotelluric and dipole-dipole resistivity data. *Geophysics* **54**, 254–262.

Sasaki Y. 2001. Full 3D inversion of electromagnetic data on PC. *Journal of Applied Geophysics* **46**, 45–54.